

Large Area Microchannel Plate Imaging Event Counting Detectors With Sub-Nanosecond Timing

O. H. W. Siegmund, *Member, IEEE*, J. B. McPhate, S. R. Jelinsky, J. V. Vallerga, A. S. Tremsin, *Member, IEEE*, R. Hemphill, H. J. Frisch, R. G. Wagner, J. Elam, A. Mane, and LAPPD COLLABORATION

Abstract—Progress towards the development of a 20 cm sealed tube optical detector with imaging and photon event time stamping is presented. Novel microchannel plates employing borosilicate micro-capillary arrays have been tested. These provide many performance characteristics typical of conventional MCPs, but have been made in sizes up to 20 cm, have low intrinsic background ($0.08 \text{ events cm}^{-2} \text{ s}^{-1}$) and very stable gain behavior for at least 7 C cm^{-2} of charge extraction. Bialkali (Na_2KSb) photocathodes with $>20\%$ quantum efficiency have also been made on 20 cm borofloat-33 windows compatible with a large sealed tube device.

Index Terms—Ionizing radiation sensors, photodetectors, radiation detectors, sensors.

I. INTRODUCTION

THE development of large area imaging and timing detectors with high performance has advantages for many potential applications, but also presents some significant challenges. For example, in the application of detection of Cherenkov light in neutrino detection, timing resolution of a few picoseconds and spatial resolution of $<1 \text{ mm}$ over areas of 20 cm would be advantageous. Currently available devices are limited to sizes of about 5 cm and use either conventional microchannel plates (MCPs), or multiple-dynodes for electron amplification, coupled to pad array readouts. Extension of these schemes to devices as large as 20 cm presents significant problems and potentially considerable cost. A collaboration (Large Area Picosecond Photon Detector, LAPPD) [1] of the University of Chicago, Argonne National Laboratory, the University of California, Berkeley, and a number of other national laboratories, universities and commercial companies

Manuscript received June 15, 2012; revised October 04, 2012; accepted January 09, 2013. Date of publication April 01, 2013; date of current version April 10, 2013. This work was supported in part by the U.S. Department of Energy under Contract DE-AC02-06CH11357 and NASA Grant NNX11AD54G. The LAPPD collaboration is based at the Argonne National Lab, Lemont, IL 94720 USA.

O. H. W. Siegmund, J. B. McPhate, S. R. Jelinsky, J. V. Vallerga, A. S. Tremsin, and R. Hemphill are with the University of California, Berkeley, Berkeley, CA 94720 USA (e-mail: ossy@ssl.berkeley.edu; mcphate@ssl.berkeley.edu; sharonj@ssl.berkeley.edu; jvv@ssl.berkeley.edu; ast@ssl.berkeley.edu; rhemp@ssl.berkeley.edu).

H. J. Frisch is with the University of Chicago, Chicago, IL 94720 USA (e-mail: frisch@hep.uchicago.edu).

R. G. Wagner, J. Elam, and A. Mane are with the Argonne National Lab, Lemont, IL 94720 USA (e-mail: rgwcdl@hep.anl.gov; jlam@anl.gov; amane@anl.gov).

Color versions of one or more of the figures in this paper are available online at <http://ieeexplore.ieee.org>.

Digital Object Identifier 10.1109/TNS.2013.2252364

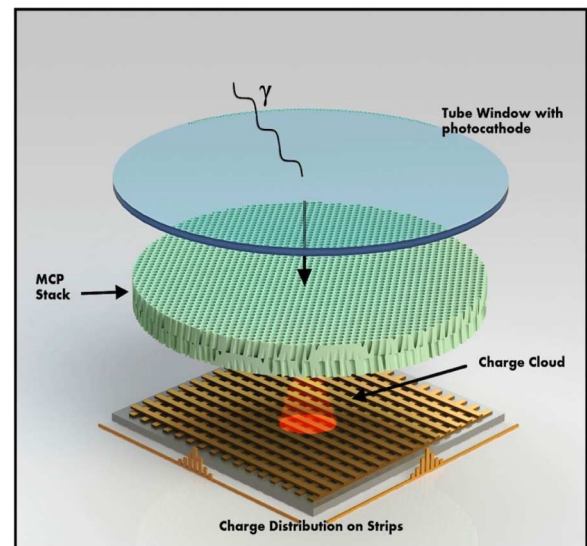


Fig. 1. Depiction of a sealed tube MCP detector. Incoming photons pass through an entrance window and are converted to photoelectrons by a semitransparent photocathode. An MCP pair (stack of 2) multiplies the photoelectron and the resulting $\sim 5 \times 10^6 e^-$ is collected by a strip-line anode.

have undertaken the task of employing novel technologies to develop a 20 cm format sealed tube visible sensitive detector.

The operational scheme of the photodetector is illustrated in Fig. 1. Incoming light passes through an entrance window (Schott Borofloat 33 [2]) and interacts with a semitransparent photocathode on the inside of the window. The photoelectrons emitted are accelerated across a proximity gap and are detected by an MCP pair. This pair of novel borosilicate substrate MCPs, that are functionalized by atomic layer deposition, amplify the signal and the resulting electron cloud is detected by a strip line anode for determination of the event positions and the time of arrival.

Development of such a device in a square 20 cm format presents challenges: hermetic sealing to a large entrance window, a 20 cm semitransparent photocathode with good efficiency and uniformity, 20 cm MCPs with reasonable cost and performance, robust construction to preserve high vacuum and withstand an atmosphere pressure differential. The development plan at the University of California, Berkeley is based on a conventional ceramic brazed assembly, while Argonne Laboratory is developing a lower-cost all-glass device. The sealed tube concept for the Berkeley effort is shown in Fig. 2. A stripline array anode on an Al_2O_3 substrate with contact pins for each stripline is brazed to an Al_2O_3 frame with a copper indium well that facilitates the hot sealing of a Schott

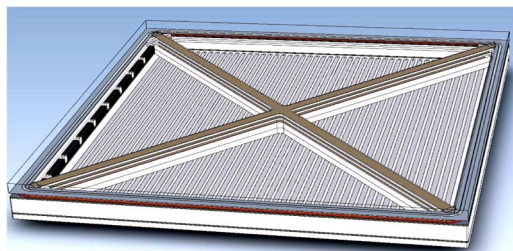


Fig. 2. Structure of a 20 cm "flat panel" microchannel plate sealed tube detector. A large borofloat-33 entrance window is indium sealed to a brazed ceramic body that has a strip-line anode readout. The microchannel plates (not shown) are clamped between "X" spacers to accommodate an atmosphere pressure differential. Getters are used to maintain high vacuum.

Borofloat 33 (borosilicate) 5 mm thick entrance window. In the final sealed tube assembly the MCPs will be spaced, and held in place by ceramic "X's" that carry the load from the front to the back of the tube for an atmosphere pressure differential. This scheme allows a thinner, lower mass window to be used, which is better for the tube assembly processes, and for scintillator to photocathode proximity. However there is a loss of effective area. High voltage contacts are made with pin feedthroughs, and getters are installed to help maintain the high vacuum in the enclosure. A bialkali photocathode was chosen as this provides reasonable sensitivity in the spectral region of interest (350 nm to 600 nm) for Cherenkov and scintillation detection and provides a low background event rate and high stability. The MCPs are based on a novel concept where the substrate is constructed from a borosilicate (700°C softening point) micro-capillary array that is made to function as an MCP by deposition of resistive and secondary emissive layers using atomic layer deposition (ALD) [3], [4]. This differs from conventional MCP lead glass construction [5], removing the need for chemical etching and H₂ reduction steps and allowing the operational parameters to be set by tailoring the sequential ALD deposition processes. The process is potentially less expensive than conventional MCPs and allows very large MCPs to be produced with pore sizes in the 10 μm to 40 μm range.

Each of the critical elements of the detector system have been evaluated to establish their performance characteristics and assess compatibility for a 20 cm sealed-tube detector. We discuss in this paper the considerable development and optimization undertaken with borosilicate ALD MCPs to achieve devices that are able to accommodate a 20 cm format.

II. BOROSILICATE MICROCHANNEL PLATES

Borosilicate micro-capillary array substrates functionalized with ALD layers to produce working MCPs require all the performance parameter optimizations customarily needed for a conventional MCP. However, in this case we can largely separate the substrate optimization and resistive/emissive layer optimization since these are sequential operations. The substrate optimization includes issues of cleanliness and debris removal, but also involves minimization of pore crushing at the hexagonal multifiber boundaries (Figs. 3, 4, and 5) and keeping the pore sizes uniform over the entire substrate.

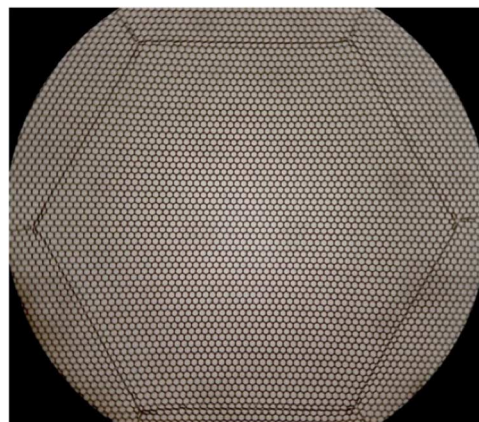


Fig. 3. Photograph of a 20 μm pore microchannel plate borosilicate substrate having 65% open area. Pore sizes are uniform except for the row adjacent to the hexagonal multifiber boundary. 1.5 mm wide area.

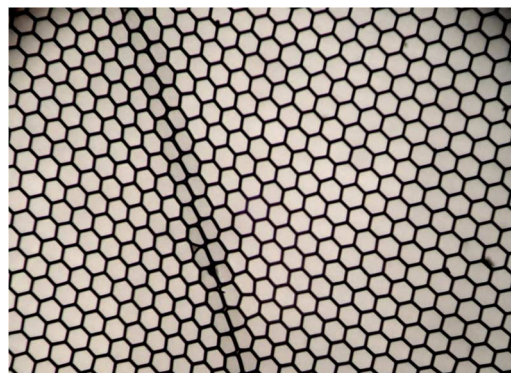


Fig. 4. Photograph of a 40 μm pore borosilicate microchannel plate having 83% open area. Several rows of pores adjacent to the hexagonal multifiber boundary are distorted. Individual pores are also hexagonal.

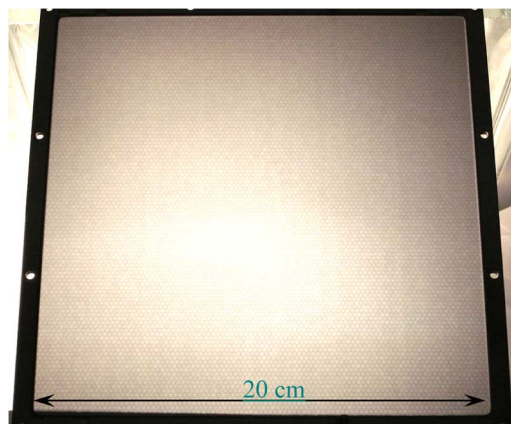


Fig. 5. Backlit photograph of a 20 cm MCP with 40 μm pores and 8° bias showing the uniformity of the multifiber stacking arrangement.

Initial substrates [6] showed pore size non-uniformity and multifiber boundary crushing that were significant, producing significant image modulation. More recent 20 μm and 40 μm pore, 33 mm substrates (Figs. 3, 4) produced by INCOM Inc. have much improved structure as seen by optical inspection. The ability to tailor the pore open area ratio, up to values of 83%

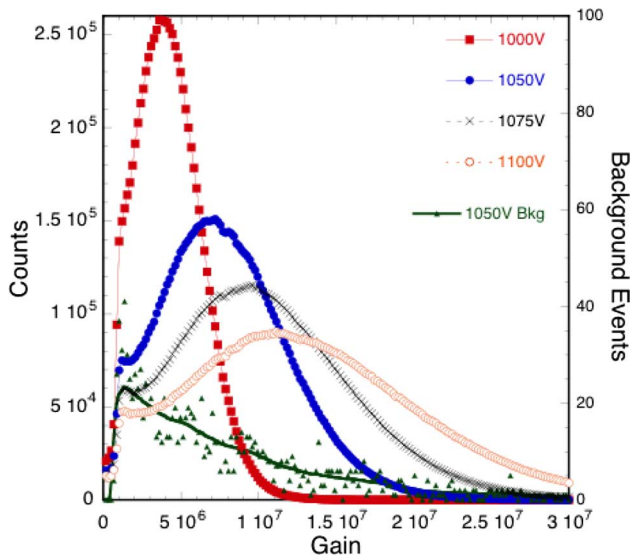


Fig. 6. Pulse height amplitude distributions for a 33 mm ALD borosilicate MCP pair. 20 μm pores, 8° bias, 60:1 L/d, 0.7 mm–300 V pair gap-bias, 185 nm illumination. 3000 sec background accumulation, 0.085 events $\text{cm}^{-2} \text{s}^{-1}$.

(Fig. 4) also has implications for the event detection efficiency. The pore uniformity is also very good for the much larger 20 cm substrates (Fig. 5) indicating that even over large areas this substrate methodology is a viable option.

In concert with the substrate optimizations, several ALD chemistries have been examined for the resistive layer application. Additionally ALD coatings of Al_2O_3 and MgO have been evaluated as the secondary emissive layer. Details of the ALD processes are discussed in more detail elsewhere [3], but significant progress has been made in matching, and sometimes exceeding, conventional MCP performance.

A. 33 mm Microchannel Plate Performance Characteristics

A significant part of the testing and optimization of the ALD borosilicate MCP development has been accomplished using 33 mm diameter MCPs. The nominal configuration has been 20 μm pore size, 60:1 pore L/d ratio and 8° pore bias angle. The majority of our evaluation tests were done in photon counting imaging detectors that employ a pair of MCPs and a cross delay line readout anode [6]. In this configuration there is a ~ 7 mm MCP output to anode gap, and the MCPs may be placed back to back, or spaced apart with a bias applied over the gap. Direct uniform illumination of the MCP with 185 nm ultraviolet (UV) light is the nominal excitation method. A number of MCPs have been tested to determine the critical performance behavior traits.

The first measurements to be done in each test are the gain as a function of applied voltage and the pulse amplitude distribution. Fig. 6 shows a typical result for a pair of ALD borosilicate MCPs with a gap between the MCPs. The gain values can exceed 10^7 with a peaked (saturated) pulse height distribution. This is close to that expected for conventional MCPs [7]–[9] with similar physical specifications. Images accumulated (Fig. 7) under 185 nm UV illumination show the overall uniformity of response is good ($\pm 10\%$, discounting the deficiencies at the multifiber boundaries). However, the hexagonal multifiber modulation of the top MCP, and faintly, the bottom

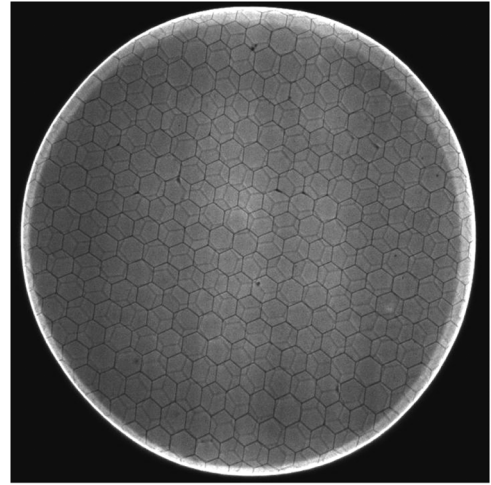


Fig. 7. Photon counting accumulated image using 185 nm illumination. ALD borosilicate MCP pair, 20 μm pore, 60:1 L/d, 8° bias, 0.7 mm/1000 V MCP pair gap/bias, at 7×10^6 gain, 1025 V bias on each MCP. Lighter color represents regions with more accumulated counts.

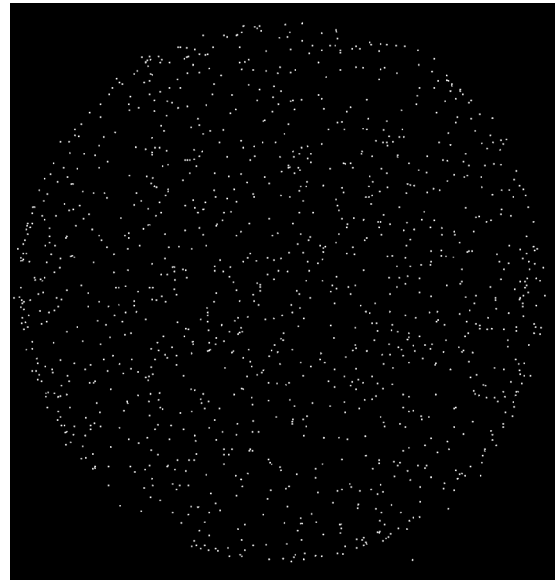


Fig. 8. Background event image. ALD borosilicate MCP pair, 20 μm pore, 60:1 L/d, 8° bias, 0.7 mm/1000 V MCP pair gap/bias, 3000 sec background, 0.085 events $\text{cm}^{-2} \text{s}^{-1}$ at 7×10^6 gain, 1050 V bias on each MCP.

MCP are both seen. A few small defects are seen close to the multifiber triple points. The image edge bright ring effect is due to field distortions related to the MCP mounting ring of the detector. An average gain image map taken at the same time shows the gain is uniform to better than 10% over the field of view. Additionally, the multifiber boundary zones have gain $\sim 15\%$ lower than other areas, presumably due to the local area crushing of pores. Considerable effort was made to reduce these multifiber distortions [10] for standard MCPs, with much success. This may also be possible for borosilicate MCPs.

The spatial distribution of background events is found to be quite uniform. Furthermore, the negative exponential distribution of background events in Fig. 8 is indicative of a source of events that is evenly distributed throughout the MCP material. However, the observed rate of 0.085 events $\text{cm}^{-2} \text{s}^{-1}$ is much

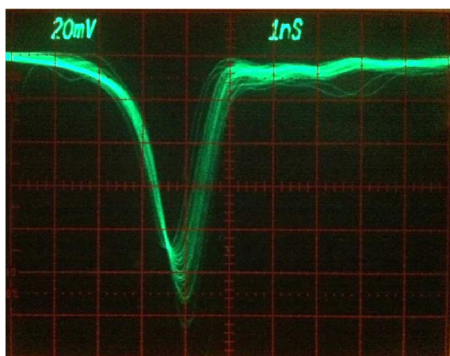


Fig. 9. Fast pulse response from single photons detected with an ALD borosilicate MCP pair, 20 μm pore, 60:1 L/d, 8° bias, 0.7 mm/1000 V MCP pair gap. Single event pulses are <1.25 ns wide.

less than conventional MCPs. This is the result of a considerable reduction in the amount of radioactive alkali (K, Rb) material in the MCP glass substrate, which dominates [9] the background rate for conventional MCPs (typically 1 to 0.25 events $\text{cm}^{-2} \text{s}^{-1}$).

The fast pulse response of single-photon amplified events was examined with a fast amplifier (150 ps risetime) and a 1 GHz analog oscilloscope. The event response of a 20 μm pore MCP pair is shown in Fig. 9 with the trigger amplitude set high to allow the pulse shape to be seen more clearly. The ~ 1.25 ns pulse width (FWHM) and pulse fall-time are comparable to conventional MCPs of the same geometry. Time tagging these events to the accuracy of the MCP signal transit time jitter [7] should provide event timing resolution to much better than 100 ps, when used with a suitable discriminator circuit.

III. PHOTOCATHODES

A. Bialkali Semitransparent Photocathodes

The deposition of large area photocathodes has been established for photomultipliers for some time. However, the implementation of large area photocathodes for sealed tube transfer photocathodes, which are required for this program, is not a well established process. The largest commercially available devices with transfer photocathodes are 150 mm (PHOTEK MCP1150 and DM150) however most devices are considerably smaller. After considering issues affecting the implementation of alkali photocathodes for 20 cm MCP-based proximity-focused sealed tubes, we have selected Na_2KSb bialkali photocathode as a viable starting material. This photocathode material has a low background rate, and high conductivity, with a high temperature tolerance compared with other bialkali photocathode types [11]. However its quantum efficiency is not as high as K_2CsSb photocathodes [11], and there is no information about its behavior with our chosen Borofloat 33 window substrate. Therefore we have initiated an evaluation of Na_2KSb bialkali photocathodes deposited on Borofloat 33 windows.

Initial tests were made by simultaneously depositing Na_2KSb semitransparent photocathodes onto four 31 mm diameter Borofloat 33 window substrates arranged within a 75 mm square area. The photocathode quantum efficiency as

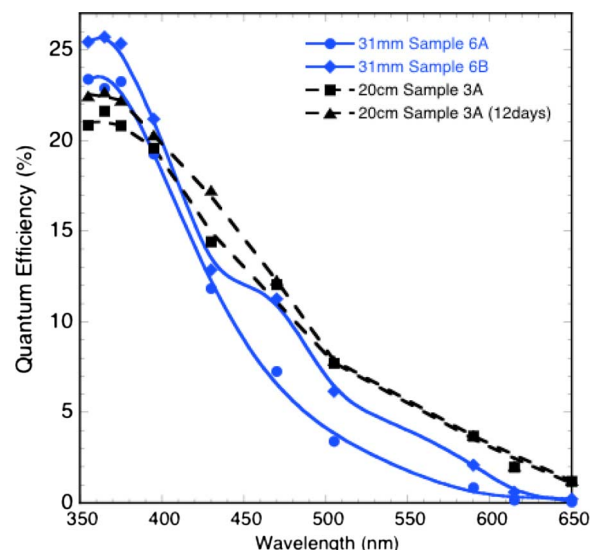


Fig. 10. Quantum efficiency for two depositions of Na_2KSb cathodes on 31 mm windows (samples 6A, 6B) and a 20 cm window (sample 3A) show good efficiency and stability for these bialkali cathodes on borosilicate windows.

a function of wavelength was measured using narrow-band LEDs (FWHM 10–50 nm), focused to a 1 cm spot. The response of the cathode was compared to the response of a NIST traceable Si photodiode to derive the quantum efficiency. No changes in the photocathode quantum efficiencies were seen over the week following deposition while the photocathodes remained at high vacuum. The wavelength dependence of the quantum efficiency is typical of Na_2KSb semitransparent photocathodes, and the quantum efficiency values achieved are comparatively high. The tests also verify the compatibility of Borofloat 33 as a good window substrate. The next verification test was to deposit a 20 cm Na_2KSb semitransparent photocathode on a 22 cm Borofloat 33 window so that the overall photocathode efficiency and uniformity over large areas could be assessed. The photocathode efficiency for this large area deposition (sample 3A) was similar to the smaller area depositions, and did not degrade over 12 days in vacuum (Fig. 10). Furthermore the measured efficiency was uniform to $\pm 15\%$ over the majority of the photocathode area (all save the extreme corners where it was difficult to measure the QE due to beam vignetting and reflections inside vacuum system). These results are encouraging in that they support the technique of window transfer and indium seal for our large area tube devices.

B. GaN Opaque Photocathodes on Microchannel Plates

Applications of MCP detectors for UV (<350 nm) sensing often use opaque photocathode layers [12] directly deposited onto the MCP surfaces to achieve the best quantum efficiency and imaging characteristics. This is normally not possible for optically sensitive photocathodes such as the bialkali and CsTe materials due to processing constraints and contamination by, and of, the MCPs.

The ALD borosilicate MCPs offer a potentially cleaner, more robust (700°C softening point) and tolerant substrate for opaque photocathode materials. We have investigated this opportunity by depositing opaque GaN (p-doped) photocathode

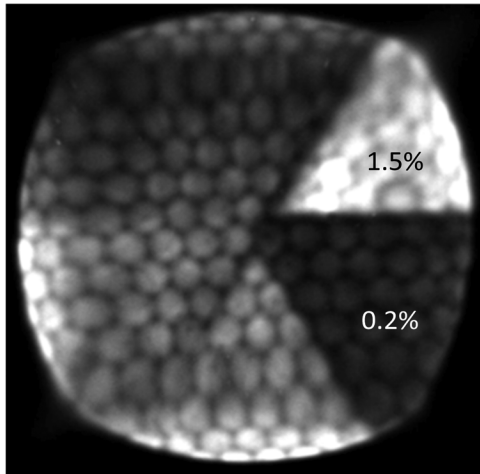


Fig. 11. Photon counting accumulated image using 185 nm (45°) illumination. ALD borosilicate MCP pair, $20\ \mu\text{m}$ pore, 60:1 L/d, 8° bias, with GaN of deposited by MBE onto the top MCP (Fig. 12). Quantum efficiency measured for the bare MCP and 300 nm GaN zone are shown. Lighter color represents regions with more accumulated counts.

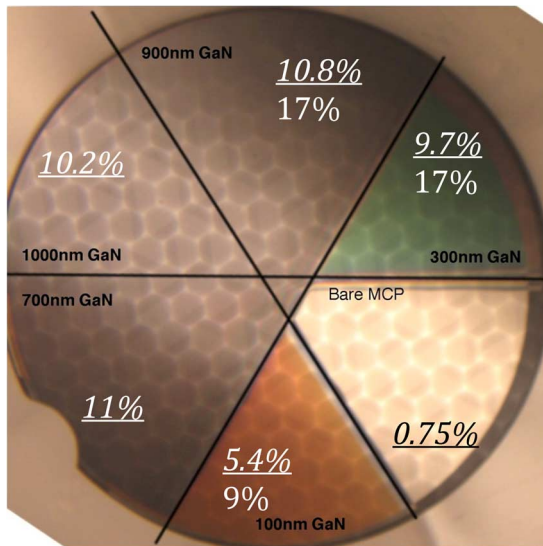


Fig. 12. ALD borosilicate MCP pair, $20\ \mu\text{m}$ pore, 60:1 L/d, 8° bias, with GaN of several thicknesses deposited by MBE onto the top MCP. Quantum efficiency for the bare MCP and GaN zones are shown, measured after Cs deposition, 10° (underlined) or 45° angle to MCP normal (214 nm UV).

onto an ALD borosilicate MCP by molecular beam epitaxy [13]. The GaN deposition was done selectively so that several different thicknesses were deposited in 6 sections of the MCP (Figs. 11, 12). One section was uncoated, exposing the MCP electrode material, while other sections had thicknesses from 100 nm up to 1000 nm. The typical p dopant concentration is of the order 10^{19} , and it is expected that the GaN penetration into the MCP pores is asymmetrical due to the pore bias angle. Since the deposition conditions are not optimal, and the substrate material was NiCr on the MCP, the surface lattice matching is poor, producing a polycrystalline/amorphous GaN layer.

For testing of this photocathode we used the GaN coated MCP as the top MCP of a pair, installed into a detector with a cross delay line photon counting imaging readout. Measurement of the relative efficiency of the, as deposited, GaN in the

MCP pores at an angle of $\sim 45^\circ$ (Fig. 11) shows a significant increase in quantum efficiency for the zone coated with 300 nm GaN. However, without Cs surface activation it is not possible to achieve optimal quantum efficiency performance. Therefore after a vacuum bake at $\sim 300^\circ\text{C}$, Cs was deposited to reduce the surface work function. Measurements of the surface (MCP web area) quantum efficiency for 214 nm light were then taken at several incident angles (Fig. 12). In the opaque photocathode configuration the quantum efficiency increases as the photocathode layer thickness increases until the layer fully attenuates the incoming radiation, or when the photoelectrons generated can no longer reach the emission surface. Thus the quantum efficiency tends to an asymptotic value as the GaN layer thickness increases as is seen in Fig. 12. Illumination at a 45° angle produces photoelectrons in the GaN closer to the emission surface (increasing the probability of transport to the surface and emission), thus the quantum efficiency values are significantly higher. The value of 17% is not as high as the 35% values achieved at the same wavelength for opaque GaN photocathodes on matched sapphire (Al_2O_3) substrates that we have measured previously [13]. However, it is significant that this level of efficiency has been achieved on a non-optimal substrate and without a Cs deposition optimization process. Al_2O_3 deposition is one of the standard ALD depositions used for the MCP fabrication process so further improvements may be possible by using ALD to deposit an Al_2O_3 film onto the top surface of the MCP prior to GaN deposition.

IV. MCP PRECONDITIONING AND LIFETIME

Implementation of MCPs in sealed tube detectors requires a number of preparatory steps. A significant concern is the evolution of gas from the MCPs and its effect on the lifetime of a sealed tube from the perspective of contamination effects, and of ion feedback damage to the photocathode. In most sealed tubes of this type precautions (preconditioning) are taken to reduce these effects, including a vacuum bake and a charge extraction “burn in” or “scrub” to minimize the gas load and to stabilize the operation of the MCPs [14]. Further precautions are also taken in some cases [15], including a thin protective layer on top of the MCP top surface, or between two MCPs in a stack, to prevent ion feedback. Although these methods are effective in reducing ion feedback they also reduce the electron detection efficiency of the detector. Generally, for conventional MCPs the gain remains the same after bake, but reduces as a function of extracted charge [14]. However, this is not usually the limiting factor on device lifetime as the gain can normally be re-established by applying higher MCP bias voltage. In conventional MCP operation a $\sim 350^\circ\text{C}$ vacuum bake followed by extraction of $\sim 0.2\ \text{C cm}^{-2}$ is adequate to reduce the gas evolution and stabilize the MCP gain [14].

We have begun the assessment of the vacuum bake and burn in characteristics of ALD borosilicate MCPs. A detector accommodating pairs of 33 mm MCPs using a cross delay line readout anode, and with all components implemented in metal or ceramic has been assembled for these tests. The first test of ALD MCP preconditioning (Fig. 13) using an early ALD formulation indicated that the gain of the ALD borosilicate MCPs (#613 & #612) did not change during the bake process. Subsequently

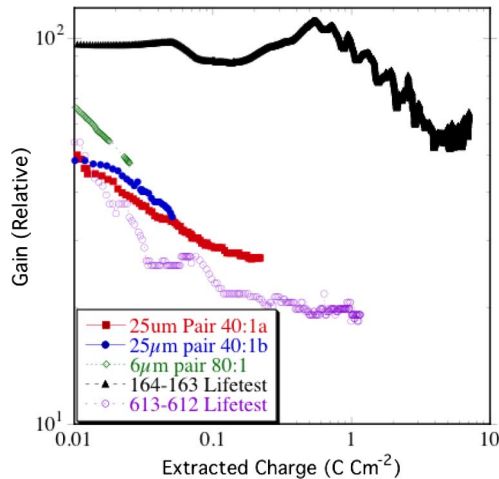


Fig. 13. Charge extraction for 33 mm ALD MCP pairs #613-612 and #164-163, ($20\ \mu\text{m}$ pore, 60:1 L/d, 8° bias) compared with conventional MCPs. Typical charge extraction rates of 1 to $3\ \mu\text{A}$, at gain of $\sim 10^5$ using UV flood.

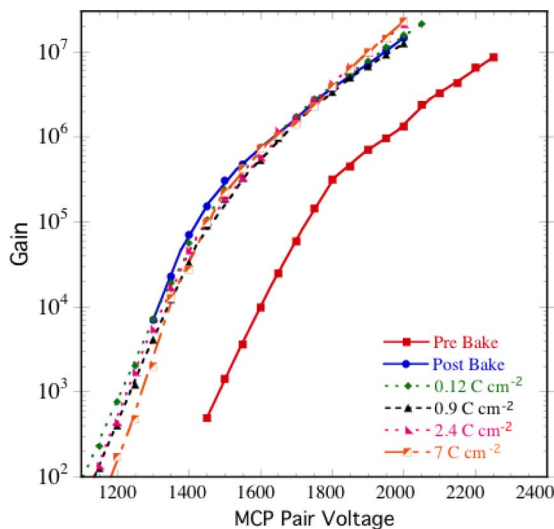


Fig. 14. Gain as a function of voltage for an ALD borosilicate MCP pair ($20\ \mu\text{m}$ pore, 60:1 L/d, 8° bias) at several stages of preconditioning operations. Significant gain increase was seen after the vacuum bake step.

the “burn-in” was very similar to that expected for conventional MCPs. The ALD materials and processes have been modified since that test, and so a second test with new MCPs was initiated. In this case a pair of MCPs (#163 & #164) was used, in a stack with a $25\ \mu\text{m}$ thick unbiased gap between them. The MCP resistances were each $\sim 150\ \text{M}\Omega$ with $20\ \mu\text{m}$ pores, 60:1 L/d and 8° bias angle. Initially the gain and imaging characteristics were assessed in the same manner as described in Section II-A, with results similar to those presented in that section.

The gain as a function of voltage characteristic is shown in Fig. 14. Prior to any pre-conditioning steps the gain reaches $\sim 10^7$ when 2250 V is applied to the pair, and the gain curve shows the onset of gain saturation at about 3×10^5 gain. After cooling following a high vacuum bake lasting ~ 40 hours and peaking at $\sim 350^\circ\text{C}$ the corresponding gain curve (Fig. 14) shows a gain increase of a factor of ~ 10 at applied MCP pair voltages above 1700 V, and increases of a factor of ~ 100 below 1600 V. Functional tests show no substantial differences in the

imaging and background behavior, no differences in the uniformity of the gain across the field of view, and no changes in the uniformity of response to UV light. Residual gas analyzer data taken during the bake shows substantial reduction in the water vapor and atmospheric gases, as is expected for a typical vacuum bake operation. Gain increase can occur as a result of surface cleaning of the ALD secondary emissive layer. The MgO secondary electron emissive layer used here shows an increase in its emission coefficient with the removal of surface contaminants [16], and this would result in the higher MCP gain.

Following the vacuum bake, a “burn-in” of the MCPs was begun (Fig. 13). The configuration used 185 nm UV full-field illumination as the input stimulation, and a gain of $\sim 3 \times 10^5$ was established resulting in an output current of $\sim 1\ \mu\text{A}$. Gas evolution was relatively low compared with conventional MCPs, with a differential pressure contribution of only a few $\times 10^{-10}$ torr attributable mainly to hydrogen evolution from the MCPs (as indicated by residual gas analysis performed continuously throughout the test). Adjusting the input UV flux, the output current was increased to $\sim 2\ \mu\text{A}$ when the extracted charge reached $0.05\ \text{C cm}^{-2}$ and to $\sim 3\ \mu\text{A}$ when the extracted charge reached $0.12\ \text{C cm}^{-2}$. The applied voltage was never adjusted. Unlike the earlier ALD MCP “burn-in” test (Fig. 13), and conventional MCP “burn-in” trends [14], the relative gain changes slowly, without a precipitous initial drop. The deviations of the gain curve are attributable to temperature changes in the laboratory, and some of the apparent gain decrease may be due to lamp flux and UV detection efficiency losses. The absolute gain calibrations (Fig. 14) at various stages show only small gain changes, with the gain (2×10^6) at 1700 V applied not changing at all over the entire $7\ \text{C cm}^{-2}$ burn-in. The lack of substantial gas evolution and gain change infers a level of cleanliness and robustness of the ALD MCP surface layers that is not seen for conventional MCPs [14]. More life tests are underway to verify our observations, and if confirmed would suggest that after the vacuum bake a substantially shorter than normal “burn-in” would be adequate. This would reduce the time and cost for making sealed tube devices.

We have also investigated the “burn-in” of another ALD MCP pair (Fig. 15) without any initial vacuum bake. Characteristics of conventional MCPs during “burn in” are the same, with or without [17] a bake. For a modest ($\sim 0.1\ \text{C cm}^{-2}$) level of charge extraction with an ALD MCP pair the gain increases by almost a factor of two, where conventional MCPs would drop by a factor of 5 (Fig. 13). Above $\sim 0.05\ \text{C cm}^{-2}$ the gain seems to stabilize. Studies of the MgO surfaces during plasma cleaning also show increases in the secondary electron emission coefficient [16]. So baking, or burn-in, both promote higher gain performance. This is a significant difference from conventional MCPs and may be advantageous in some applications.

V. 20 cm BOROSILICATE ALD MCP TESTS

A number of 20 cm square borosilicate substrate MCPs have been fully ALD functionalized, both in $40\ \mu\text{m}$ and $20\ \mu\text{m}$ pore sizes. We have been able to test pairs of MCPs in a detector designed to perform photon counting imaging tests by employing a large cross delay line anode readout (Fig. 16). The MCPs

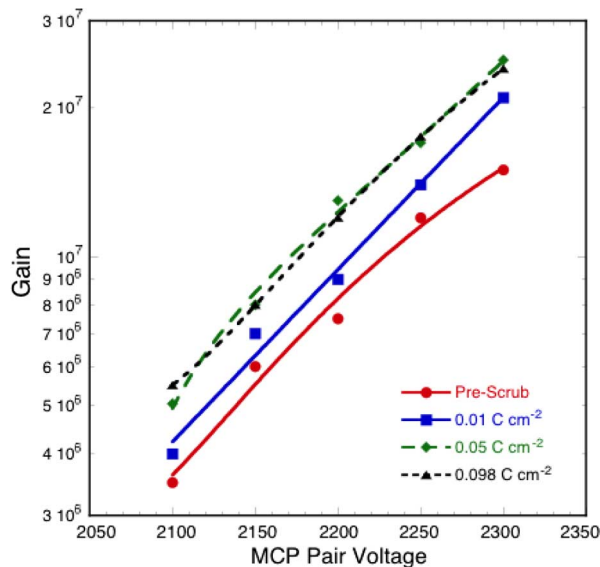


Fig. 15. Charge extraction for a 33 mm ALD MCP pair (20 μm pore, 60:1 L/d, 8° bias). Charge extraction rate of $\sim 1 \mu\text{A}$, at gain of $\sim 10^5$ using UV flood.

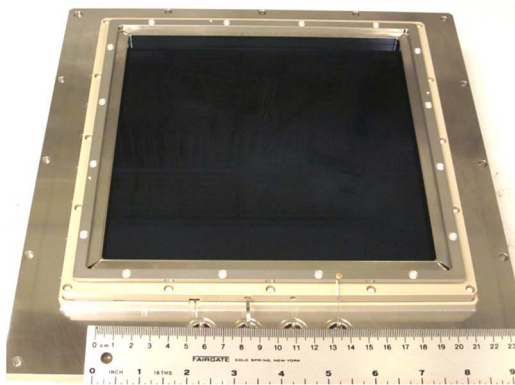


Fig. 16. 20 cm ALD 20 μm pore, 60:1 L/d, 8° bias MCP pair in a detector assembly with a cross delay line imaging readout for photon counting tests.

are spring clamped around the periphery, and have a 0.7 mm insulating spacer between them that allows a bias to be applied to this inter-MCP gap. There is a 12 mm MCP to anode gap to allow the charge cloud to spread before impacting the anode. A cross delay line serpentine anode [18] with a 20×20 cm active area is used for the imaging readout. The serpentine period is 4 mm with equal charge sharing between the upper and lower orthogonal serpentes. End-to-end delay times are ~ 100 ns to permit high overall event rate encoding and spatial resolution $> 4 \text{ k} \times 4 \text{ k}$ pixels.

A number of 20 cm MCP pairs were tested, with 20 μm pores, 60:1 L/d, 8° bias and resistances ranging from 1 M Ω to 80 M Ω . A 200 V inter-MCP gap bias was applied, and a 100 V MCP to anode bias. 185 nm UV light illuminated the entire detector with detected event rates of 30 kHz–200 kHz. The highest average gain achieved was of the order 2×10^7 with individual MCP biases of ~ 1150 V. The pulse amplitude distributions are similar to the ones obtained for the 33 mm MCPs (Fig. 7). An image of the UV response of an MCP pair, which was obtained by accumulating $\sim 4 \times 10^8$ events, is shown in Fig. 17. The

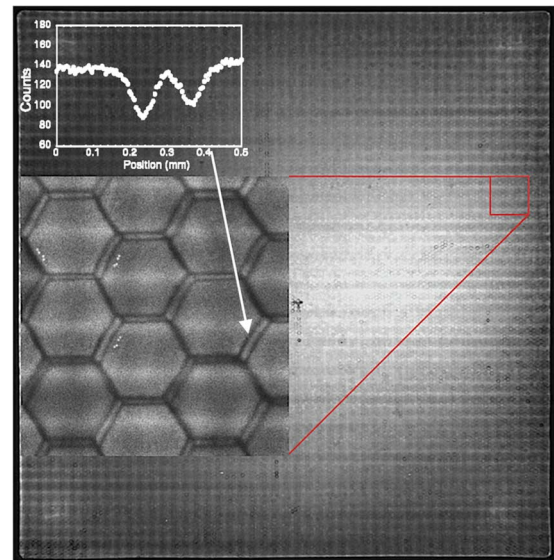


Fig. 17. Photon counting image (4 k \times 4 k bins) accumulation for a 20 cm, 20 μm pore, 60:1 L/d ALD-MCP pair, 0.7 mm pair gap 200 v, using 185 nm UV illumination. Lighter color indicates more accumulated counts. The overall striping in X and Y are due to the detector readout anode periodicity of 4 mm. The inset shows an expanded area revealing the imaging of multifiber structure of the MCPs and a histogram showing $< 100 \mu\text{m}$ spatial resolution.

striations in X and Y are modulations due to the anode period, indicating that the charge spreading on the anode is not optimal. Adjustment of the MCP-anode gap and gap bias would improve this behavior. A magnified inset shows the local area detail in one zone. The multifiber structure is clearly visible for both the upper and lower MCP of the pair, as it is on the smaller 33 mm MCPs (Fig. 7). Spatial histograms of the features in Fig. 17 indicate that the spatial resolution of the detector system is better than 100 μm FWHM (2 k \times 2 k resolution elements).

Overall, the average gain of the 20 cm MCP pair varies by up to a factor of two from the center to the edge of the MCP. This causes an apparent sensitivity drop off (Fig. 17) due to the loss of low amplitude events below the electronics processing threshold. However, the gain uniformity has been consistently improving with maturation of the fabrication processes. Locally the gain is approximately 15% lower at the multifiber boundaries due to the crushing of the MCP pores at these interfaces (Fig. 5).

The background event spatial distribution for a 20 cm MCP pair is shown in Fig. 18. The most obvious features are a few “warm” spots and patches of higher event rate. Nevertheless the total background rate is $< 0.078 \text{ events cm}^{-2} \text{ s}^{-1}$ averaged over the 400 cm^2 field of view (Fig. 18). The “warm” spots are field emission from debris on the surface of the top MCP, which is being resolved by better handling and cleaning processes. More than 20 MCPs have been tested to date, with similar ($< 0.15 \text{ events cm}^{-2} \text{ s}^{-1}$) overall background rates for the more recent MCPs. This compares to 1–2 $\text{events cm}^{-2} \text{ s}^{-1}$ for MCP fabricated earlier in the project.

The intrinsic background is comparable to the values seen on the 33 mm ALD borosilicate MCPs (Fig. 9), and is considerably lower than conventional MCPs [9]. The background rate is commensurate with a $3 \times$ to $4 \times$ reduction in the radioactive



Fig. 18. Background event image accumulation (1000 sec) for a 20 cm, 20 μm pore, 60:1 L/d ALD-MCP pair, 0.7 mm pair gap 400 v, gain $\sim 1 \times 10^7$. Overall background 31 events sec^{-1} including the observed patches and “warm spots”, resulting an average rate of 0.078 events $\text{cm}^{-2} \text{sec}^{-1}$.

alkali metal content of the borosilicate glass compared to conventional MCP lead glasses. For a 20 cm MCP alone the Fig. 18 overall background rate is 31 events s^{-1} . However, the expected background rate generated by a bialkali photocathode in a sealed tube device 20 cm in size is ~ 5 kHz, so the MCP contribution is effectively negligible.

The 20 cm MCPs were operated over periods of many hours without issues, and the 33 mm MCPs were operated for more than 5 months during the life testing. Even though the resistance of some of the 20 cm MCPs was $< 5 \text{ M}\Omega$ and the current through the pair was over 200 μA , stabilization was reached in a fairly short period (10 min). So this new MCP method is functionally stable, and has specific properties (size, background, long term stability) that are attractive for some applications. More work is underway to minimize the gain variations that are a result of the non-uniformity of the ALD layer coatings and distortions of the substrate structure. Optimization and process adjustments should subsequently provide better MCP performance behavior, but even without these improvements the ALD functionalized borosilicate substrate MCPs are a viable alternative to conventional MCPs.

VI. DISCUSSION AND FUTURE WORK

Significant progress has been made towards the production of a 20 cm sealed tube optical photodetector with imaging and time stamping capabilities. Novel MCPs have been manufactured, in 33 mm diameter and 20 cm square formats, using ALD techniques to functionalize borosilicate microcapillary substrates. These MCPs have shown good imaging and low background rates over areas much larger than conventional MCPs, however more work is needed to improve the overall gain uniformity. Initial testing of ALD MCPs have demonstrated low outgassing and excellent gain stability when going through standard preconditioning steps used for the fabrication of sealed tube de-

vices. Potential implications for use in sealed tube photo-detectors are shorter processing times and potentially longer MCP and photocathode lifetimes [15]. In addition, our demonstration of deposition of opaque GaN photocathodes directly onto the ALD MCPs, offers the possibility for high efficiency UV photodetectors ($< 350 \text{ nm}$) with high spatial resolution and tolerance to high magnetic fields.

In preparation for implementation of a large sealed tube device we have deposited 20 cm, semitransparent bialkali photocathodes on the borosilicate window material we will employ for the final sealed tube. These cathodes have demonstrated good uniformity, high QE, and good stability at vacuum. Implementation of these technologies into a 20 cm sealed tube photodetector is underway, and the detector structure (Fig. 2) is close to completion. Further work in testing and optimization of ALD MCPs is also in progress to establish and take advantage of the characteristics presented in this paper.

ACKNOWLEDGMENT

The authors would like to thank the members of the team at INCOM Inc., Arradance Inc., Dr. A. Dabiran at SVT Associates, Mr. J. Hull, and Mr. J. Tedesco for their contributions to this work.

REFERENCES

- [1] [Online]. Available: <http://psec.uchicago.edu>
- [2] [Online]. Available: <http://www.schott.com/borofloat>
- [3] A. Mane, Q. Peng, J. W. Elam, D. C. Bennis, C. A. Craven, M. A. DeTarando, J. R. Escolás, H. J. Frisch, S. J. Jokela, J. McPhate, M. J. Minot, O. H. W. Siegmund, J. M. Renaud, R. G. Wagner, and M. J. Wetstein, “A novel atomic layer deposition method to fabricate economical and robust large area microchannel plates for photodetectors,” *Phys. Procedia*, vol. 37, pp. 722–732, 2012.
- [4] M. Ritala and M. Leskelä, “Atomic layer epitaxy—A valuable tool for nanotechnology?,” *Nanotechnology*, vol. 10, no. 1, pp. 19–24, 1999.
- [5] M. Lampton, “The microchannel image intensifier,” *Sci. Amer.*, vol. 245, pp. 62–71, 1981.
- [6] O. H. W. Siegmund, J. B. McPhate, J. V. Vallerger, A. S. Tremsin, S. R. Jelinsky, and H. J. Frisch, “Novel large format sealed tube microchannel plate detectors for Cherenkov timing and imaging,” *Nucl. Instrum. Methods Phys. Res. A*, vol. 639, no. 1, pp. 165–168, 2011.
- [7] O. Siegmund, J. Vallerger, P. Jelinsky, X. Michalet, and S. Weiss, “Cross delay line detectors for high time resolution astronomical polarimetry and biological fluorescence imaging,” in *Proc. IEEE Nuclear Science Symp.*, 2005, pp. 448–452, 0-7803-9222-1.
- [8] J. L. Wisa, “Microchannel plate detectors,” *Nucl. Instrum. Methods*, vol. 162, pp. 587–601, 1979.
- [9] O. H. W. Siegmund, *Methods of Vacuum Ultraviolet Physics*, J. A. R. Samson and D. L. Ederer, Eds., 2nd ed. New York, NY, USA: Academic, 1998, ch. III.
- [10] O. H. W. Siegmund, J. Vallerger, A. Tremsin, and J. McPhate, “Microchannel plates: Recent advances in performance,” *Proc. SPIE*, vol. 6686, 2007, 66860W.
- [11] A. V. Lyashenko, A. Breskin, R. Chechik, J. M. F. Dos Santos, F. D. Amaro, and J. F. C. A. Veloso, “Development of high-gain gaseous photomultipliers for the visible spectral range,” *J. Instrum.*, vol. 4, 2009, P07005.
- [12] O. H. W. Siegmund, B. Y. Welsh, J. V. Vallerger, A. S. Tremsin, and J. B. McPhate, “High-performance microchannel plate imaging photon counters for spaceborne sensing,” *Proc. SPIE*, vol. 6220, 2006.
- [13] O. H. W. Siegmund, A. S. Tremsin, J. V. Vallerger, J. B. McPhate, J. S. Hull, J. Malloy, and A. M. Dabiran, “Gallium nitride photocathode development for imaging detectors,” *Proc. SPIE*, vol. 7021, p. 40, 2008.
- [14] O. H. W. Siegmund, “Preconditioning of microchannel plate stacks,” *Proc. SPIE*, vol. 1072, pp. 111–118, 1989.
- [15] F. Uhlig, A. Britting, W. Eyrich, and A. Lehmann, “Systematic studies of microchannel plate PMTs,” *Nucl. Instrum. Methods Phys. Res. A*, accepted for publication.

- [16] S. J. Jokela, I. V. Veryovkina, A. V. Zinoveva, J. W. Elam, A. U. Mane, Q. Peng, and Z. Insepov, LAPPD Collaboration, "Secondary electron yield of emissive materials for large-area micro-channel plate detectors: Surface composition and film thickness dependencies," *Phys. Procedia*, vol. 37, pp. 740–747, 2012.
- [17] A. Martin, J. Vallerger, J. McPhate, and O. Siegmund, "Further scrubbing and quantum efficiency results of the HST-COS far ultraviolet detector," *Proc. SPIE*, vol. 4854, pp. 526–531, 2003.
- [18] O. H. W. Siegmund, J. V. Vallerger, B. Welsh, J. McPhate, and A. Tremsin, "High speed optical imaging photon counting microchannel plate detectors for astronomical and space sensing applications," in *Proc. Advanced Maui Optical and Space Surveillance Technologies Conf.*, 2009, p. 90.